BRILL

Multidiscipline Modeling in Mat. and Str.4(2008)XX -XX

MMMS
www.brill.nl/mmms

DERIVATION AND VALIDATION OF A MATERIAL MODELFOR CLAYEY SAND FOR USE INLANDMINE DETONATION COMPUTATIONAL ANALYSES

[1]M. Grujicic, B. Pandurangan, N. Coutris,
[2]B. A. Cheeseman, W. N. Roy and R. R. Skaggs
[1]Department of Mechanical EngineeringClemson University, Clemson SC 29634
[2]Army Research Laboratory – Survivability Materials Branch, Aberdeen, Proving Ground, MD 21005-5069
mica.grujicic@ces.clemson.edu

Received 21 March 2007; accepted 28 April 2007

Abstract

A large-strain/high-deformation rate model for clay-free sand recently proposed and validated in our work [1,2], has been extended to sand containing relatively small (< 15vol.%) of clay and having various levels of saturation with water. The model includes an equation of state which represents the material response under hydrostatic pressure, a strength model which captures material behavior under elastic-plastic conditions and a failure model which defines conditions and laws for the initiation and evolution of damage/failure in the material. The model was validated by comparing the computational results associated with detonation of a landmine in clayey sand (at different levels of saturation with water) with their computational counterparts.

Keywords
Sand, Material Model, Detonation, Shallow Buried Landmine, Blast Loading

NOMENCLATURE

α_0	Initial porosity
β	Saturation ratio
B	Compaction modulus
G	Shear modulus
K	Bulk modulus
μ	Friction coefficient
Ω	Clay content
P	Pressure
ρ	Density
σ	Yield stress
τ	Shear failure pressure

Report Documentation Page

Form Approved
OMB No. 0704-0188

1. REPORT DATE	2. REPORT TYPE	3. DATES COVERED
2008		**00-00-2008 to 00-00-2008**

4. TITLE AND SUBTITLE	5a. CONTRACT NUMBER
Derivation and Validation of a Material Modelfor Clayey Sand for Use in Landmine Detonation Computational Analyses	5b. GRANT NUMBER
	5c. PROGRAM ELEMENT NUMBER
6. AUTHOR(S)	5d. PROJECT NUMBER
	5e. TASK NUMBER
	5f. WORK UNIT NUMBER
7. PERFORMING ORGANIZATION NAME(S) AND ADDRESS(ES) **Celmson University,Department of Mechanical Engineering,Clemson,SC,29634**	8. PERFORMING ORGANIZATION REPORT NUMBER
9. SPONSORING/MONITORING AGENCY NAME(S) AND ADDRESS(ES)	10. SPONSOR/MONITOR'S ACRONYM(S)
	11. SPONSOR/MONITOR'S REPORT NUMBER(S)

12. DISTRIBUTION/AVAILABILITY STATEMENT
Approved for public release; distribution unlimited

13. SUPPLEMENTARY NOTES

14. ABSTRACT

A large-strain/high-deformation rate model for clay-free sand recently proposed and validated in our work [1,2], has been extended to sand containing relatively small (< 15vol.%) of clay and having various levels of saturation with water. The model includes an equation of state which represents the material response under hydrostatic pressure, a strength model which captures material behavior under elastic-plastic conditions and a failure model which defines conditions and laws for the initiation and evolution of damage/failure in the material. The model was validated by comparing the computational results associated with detonation of a landmine in clayey sand (at different levels of saturation with water) with their computational counterparts.

15. SUBJECT TERMS

16. SECURITY CLASSIFICATION OF:			17. LIMITATION OF ABSTRACT	18. NUMBER OF PAGES	19a. NAME OF RESPONSIBLE PERSON
a. REPORT **unclassified**	b. ABSTRACT **unclassified**	c. THIS PAGE **unclassified**	**Same as Report (SAR)**	**34**	

V	Volume

Subscripts

adhesion	Adhesion strength
air	Air related quantity
clay	Clay related quantity
Comp	Value at full compaction
drysand	Dry Sand quantity
fail	Failure related quantity
MC	Mohr-Coulomb value
o	Initial value
ref	Fully-compacted sand related quantity
sand	Sand related quantity
sat	Saturation related quantity
unsat	Unsaturated Sand related quantity
water	Water related quantity

1. Introduction

Despite the signing of Mine Ban treaty in 1999, it is widely recognized that there is a landmine crisis. The following are some of the main aspects of this crisis: (a) in excess of 100 Million unexploded landmines remain deployed in over 60 countries or over the world [3]; (b) Nearly 30,000 civilians are killed or maimed every year by unintended detonations of the mines [4]; (c) the cost of medical treatment of landmine injuries exceed 100 million per year [5]; (d) the ability of the international community to provide the humanitarian relief in terms of medical services, safe drinking water and food, etc., is greatly hampered by landmine contamination of the infrastructure in mine affected countries [5]; and so on. To address the aforementioned landmine crisis, the research community around the world has taken upon itself the challenge of helping better understand the key phenomena associated with landmine detonation and interaction between detonation products, mine fragments and soil ejecta with the targets (people, structures and vehicles). Such improved understanding will help automotive manufacturers to design and fabricate personnel carriers with higher landmine-detonation survivability characteristics and a larger level of protection for the onboard personnel. In addition, the manufacturer of demining equipment and personnel protection gear used in landmine clearing are expected to benefit from a better understanding of the landmine detonation-related phenomena.

The landmine detonation related research activity can be broadly divided into three main categories: (a) shock and blast wave mechanics and dynamics including landmine detonation phenomena and large-deformation/high-deformation rate constitutive models for the attendant materials (high explosive, air, soil, etc.); (b) the kinematic and structural response of the target to blast loading including the role of target design and use of blast attenuation materials; and (c) vulnerability of human beings to post-detonation phenomena such as high blast pressures, spall fragments and large vertical and lateral accelerations.

The present work falls primarily into the category (a) of the research listed above since it emphasizes the development of a large-deformation/high-deformation rate material model for clay-containing sand with various levels of water content. It is generally recognized that the properties of soil, into which a landmine is buried, play an

important role in the overall effectiveness/lethality of the landmine regarding of the nature of its deployment (fully-buried, flush-buried or ground-laid). The present work, during the material-model validation stage, also addresses briefly the category (b) of the landmine detonation related research.

While there are a variety of soils, it is customary to divide soil into two main categories: (a) Cohesion-less soils (e.g. sand) which consist of relatively coarse particles (average particle size 4.0-4.75mm) which have a negligible tensile strength and derive their shear strength primarily from the inter-particle friction; and (b) Cohesive soils (e.g. clay) which consist of fine particles (average particle size 50-75μm) which derive their strength and failure properties from the inter- and intra-particle electrostatic and polar forces. In the present work, we address the problem of material model derivation and validation for sand containing minor (< 15vol. %) of clay. Such sand was assumed to have been at some point fully saturated with water which has caused the clay particles to become suspended in water and (upon a subsequent decrease in the water content) form a continuous (bonding) coating over the sand particles. Such sand, as will be discussed in next section, acts as a cohesive soil and displays a combination of properties derived from those of sand and clay. It should be also noted that, in addition to clay, sand may often contain silt with micron-size particles. In such cases, clay would normally act as a binder and promote formation of the agglomerates of silt particles. Such agglomerates are generally smaller than and tend to primarily reside within the sand inter-particle spaces (voids) and, hence, are not expected to have as pronounced effect on the mechanical response of sand as does clay. That is the reason why, in this work, the effect of silt is not considered.

A review of the literature shows that there exists an extensive body of work dealing with the investigation of the detonation of the buried charges. However, much of this work does not focus on the characterization of the blast output of landmines, but rather on cratering effects in soils, with applications towards the efficient utilization of explosives for excavation (i.e. canals, trenches, etc.) or in the survivability of structures subjected to near surface blasts [6]. Westine et al. [7] carried out experiments on a plate which was mounted above a buried charge comparable is size and power to an anti-tank landmine. The plate contained a number of through-the-thickness holes at incremental distances from the mine, in which, plugs of known mass were placed. The blast accompanying mine detonation caused the plugs to be ejected from the holes and from their initial velocity the impulsive loading on the plate was calculated. Morris [8] used the results of Westine et al. [7] to construct a design-for-survivability computer code for lightweight vehicles. More recently, Bergeron et al. [9] carried out a comprehensive investigation of the buried landmine blasts using an instrumented ballistic pendulum. From these experiments, the pressure and impulse as a function of time were recorded at several locations in air directly above the mine as well as in the sand surrounding the landmine, along with X-ray radiographs and high-speed photographs of the associated soil cratering and ejecting phenomena.

In our recent computational work [10], based on the use of AUTODYN, a general-purpose transient non-linear dynamics explicit simulation software [11], a detailed comparison was made between the experimental results of Bergeron et al. [12] and their computational counterparts for a number of detonation-related phenomena such as the temporal evolutions of the shape and size of the over-burden sand bubbles and of the detonation-products gas clouds, the temporal evolutions of the side-on pressures in the

sand and in air, etc. It was found that the most critical factor hampering a better agreement between the experiment and computational analysis is an inadequacy of the current material model for sand to capture the dynamic response of this material under blast loading conditions. Hence, the main objective of our subsequent work [1] was to improve the compaction material model for sand in order to include the effects of the degree of saturation and rate of deformation, the two important effects which were neglected in the original compaction model (proposed by Laine and Sandvik [13]) used in AUTODYN [11]. The new material constitutive model for sand was subsequently validated for the case of sand with different levels of (water) saturation by comparing the experimental results associated with detonation of the shallow-buried and ground-laid C4 mines obtained through the use of an instrumented horizontal mine-impulse pendulum with their computational counterparts obtained via detailed numerical modeling of the same physical problem using AUTODYN. In our subsequent work [2], the ability of the newly developed material model to predict the temporal evolutions of the blast loads associated with the detonation of mines buried in fully water-saturated sand was tested. This was done by comparing the model predictions with their experimental counterparts obtained in the work of Taylor and Skaggs [14] who carried out large-scale experiments using the *Vertical Impulse Measurement Fixture* (VIMF) at the Army Research Laboratory, Aberdeen, MD. All this work culminated in the development of a large deformation/high-deformation rate material model for sand [2]. This model for sand is referred to as CU-ARL sand model in the remainder of this manuscript.

As discussed above, the CU-ARL sand model was found to significantly improve the agreement between the transient non-linear dynamics simulations and experimental investigations of several scenarios involving detonation of landmines ground laid or buried in sand to various depths. These improvements were brought about by the inclusion of the effects of water-saturation levels on the compressibility as well as on the cohesive and shear strengths of sand. The objective of the present work is to extend the approach used in our previous work [1, 2] to the development of a material model for clay-containing sand at different levels of saturation with water. Since this model was jointly developed by Clemson University and the Army Research Laboratory, Aberdeen Proving Ground, MD, it will be referred to, in the remainder of this document, as the CU-ARL clayey-sand model. As will be shown in the next section, the mechanical response of clayey-sand is greatly affected by the phenomena such as clay-coating cohesive and shear strengths, sand inter-particle adhesion, sand inter-particle friction and the adsorption of water by the clay coating and the extent of water in the inter-particles spaces.

The organization of the paper is as follows. Morphology and microstructure of clay and clayey sand are discussed in Section II.1 and II.2, respectively. Derivation and parameterization of the CU-ARL clayey sand model are discussed in Section II.3. The results of the model validation via comparison of the computational and experimental results for a number of scenarios involving landmine detonation in sand and subsequent interactions of the detonation products, mine fragments and soil ejecta are presented and discussed in Section III. A brief summary and the conclusions obtained in the present work are discussed in Section IV.

2. Model Derivation and Computational Analysis

2.1 Atomic-level Microstructure and Morphology of Clay

As stated earlier, soils are generally classified into two groups: (a) those dominated by sand and (b) those consisting of major fractions of clay. While in both cases, the basic architecture of soil involves a skeleton of solid particles and interconnected spaces (voids) filled with air and/or water, the nature of the inter-particle forces differs in the two cases: (a) In the case of sand, very little adhesion exists between contacting particles which can interact only via mechanical/frictional forces and (b) In clays, particles are finer and more plate-like ensuring large inter-particle contact which in conjunction with the inter-particle electro-chemical forces provides a high cohesive strength and ductile behavior of the material. These properties of clay are closely related to their atomic level structure which is displayed schematically in Figure 1.

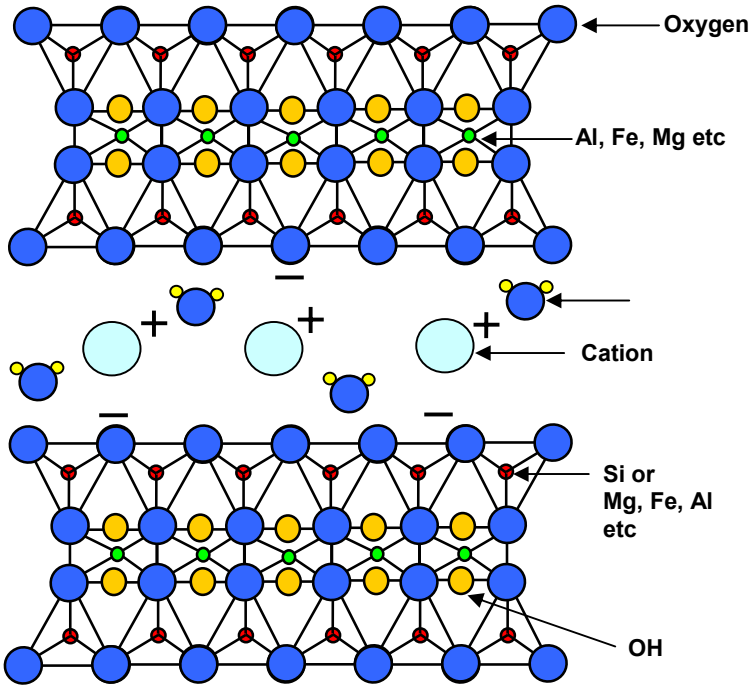

Fig.1 A schematic of the atomic-level microstructure of clay.

A simple analysis of the atomic-level microstructure of clay displayed in Figure 1 reveals that this material is composed of sheet-like silicate layers with a particular stacking sequence. In natural clay, this sequence involves a central layer consisting mainly of aluminum cations (and oxygen anions) sandwiched between two tetrahedral layers consisting of silicon cations and oxygen anions. Typically, some of the aluminum and silicon ions are replaced by lower valence ions such as Mg^{2+}, Ca^{2+}, and Li^{+} etc. creating a negative charge imbalance in each of the 3-layer sheets. The charge imbalance is neutralized by adsorption of Na^{+}, Ca^{2+} and K^{+} cations which tend to have water molecules associated with them. The hydrated Na^{+}, Ca^{2+} and K^{+} cations reside in the

interlayer region making clay behave as a pliable material and, at higher water levels, cause the clay to swell.

The atomic structure and properties of clay discussed above are expected to affect the mechanical response of sand whose particles are coated with a thin layer of clay, i.e. the type of clayey sand analyzed in the present work.

2.2 Atomic-level Microstructure and Morphology of Clayey Sand

The CU-ARL clayey sand model developed in the present work is aimed at capturing the high-deformation rate behavior of sand containing no more than 15vol.% clay. Under such conditions, clay is most frequently present as a coating on sand particles (rather than being in the form of discrete particles).

2.3 Material Model Development for Clayey Sand

As discussed earlier, the main objective of the present work is to derive a material for clayey sand with various levels of water content. Such model is needed in computational analyses of various scenarios involving landmine detonation with various types of deployments in soil. Since the computational analyses in question are of a transient, non-linear dynamic nature, the clay model to be developed (the CU-ARL clayey sand model) is primarily required to compute the response of this material under large deformation, high-deformation rate and large pressure conditions. The validity of the model under slow-speed quasi-static conditions is not the subject of this work. As discussed in our previous work [1, 2], a typical transient non-linear dynamics problem involves numerical simulation of the governing mass, momentum and energy conservation equations. Spatial coordinates and time are independent variables while mass density, velocities and the internal energy densities are the dependent variables in these equations. Since the stress appears explicitly in these equations, a set of relations (the material model) is needed to establish (for a given material) the relationships between stress and the dependent variables (and/or there integrals). Furthermore, since stress, σ, is generally decomposed into a hydrostatic stress ($-pI$, where p is pressure and I is a second order identity tensor) and a deviatoric stress σ_d, the material model is generally decomposed into: (a) an *Equation of State*, EOS (defines the density and internal energy density dependences of pressure); (b) a strength model (used to express the evolution of deviatoric stress in the elastic and elastic-plastic region of the material) and (c) a failure model (defines the damage/failure response of the material). In addition to these relations, an erosion model is often defined to alleviate numerical difficulties arising in regions experiencing large deformations. Within the erosion model, heavily deformed regions can be removed while conserving their momenta via the retention of the associated nodes as well as the nodal masses and velocities. In the remainder of the section, a brief overview is presented of the derivation of an equation of state, a strength model, a failure model and an erosion model for clayey sand.

For the microstructure of clayey sand, one would expect that the compaction/compression behavior (as represented by the equation of state) will not be significantly different than that in CU-ARL sand. On the other hand, the shear and failure behavior which are controlled by a low shear resistance and high cohesion strength of clay, respectively, will be significantly affected.

Since the CU-ARL clayey sand material model is intended to include the effects of porosity, degree of saturation and clay content, following parameters are defined to represent the chemical and microstructural state of sand:

$$\alpha = \frac{V_{water} + V_{air}}{V_{total}} \tag{1}$$

$$\beta = \frac{V_{water}}{V_{water} + V_{air}} \tag{2}$$

and

$$\Omega = \frac{V_{clay}}{V_{clay} + V_{sand}} \tag{3}$$

where α is the extent of porosity, β is the degree of saturation, Ω is the solid fraction of clay (clay content), V is the volume and the subscripts *sand*, *clay*, *air*, *water* and *total* are self explanatory.

CU-ARL Clayey-sand Equation of State

In this section, the equation of state (EOS) representing the compaction behavior of clayey sand is presented. Table 1 contains a list of all parameters appearing in the equation of state for the dry, unsaturated and saturated clayey sands. The equation of state for the CU-ARL clayey sand is defined below as a simple extension of the CU-ARL sand EOS to account for the effect of clay on the model parameters. The CU-ARL sand EOS was originally derived by separately developing the equation of state for dry and fully saturated sand and combining them (using a simple rule of mixture) to define the corresponding relationships for unsaturated sand [2].

Table 1. Parameters appearing in the definition of EOS model for dry, unsaturated and saturated clayey sands with an initial porosity of 0.36 and a clay content of 0.15.

Parameter	Symbol	Unit	Value
Dry Clayey Sand			
Initial Density of Dry Clayey Sand	$\rho_{0,dry\ clayey\ sand}$	kg.m^{-3}	1637.2
Reference Density of Dry Clayey Sand	$\rho_{s,\ dry\ clayey\ sand}$	kg.m^{-3}	2558.2
Dry Clayey Sand Plastic Compaction Modulus	$B_{PlComp,\ dry\ clayey\ sand}$	MPa.m.^{3}kg^{-1}	581.66
Dry Clayey Sand Solid Compaction Modulus	$B_{SolidComp,\ dry\ clayey\ sand}$	MPa.m.^{3}kg^{-1}	18453
Minimum Pressure for Full Compaction of Dry Clayey Sand	$P_{Comp,\ dry\ clayey\ sand}$	GPa	0.5531
Saturated Clayey Sand			
Initial Density ofSaturated Clayey Sand	$\rho_{0,sat\ clayey\ sand}$	kg.m^{-3}	1997.2
Saturated Clayey Sand Compaction Modulus	$B_{Comp,\ sat\ clayey\ sand}$	MPa.m.^{3}kg^{-1}	12584
Minimum Pressure for Full Compaction of saturated Clayey Sand	$P_{Comp,\ sat\ clayey\ sand}$	GPa	0.5531

Dry Sand: The relevant CU-ARL dry sand EOS relations are presented first. The dry-sand pressure dependence on density is defined as [1]:

$$P_{dry\,sand}=\begin{cases}0 & \rho_{dry\,sand}\le\rho_{o,dry\,sand}\\ B_{Pl.Comp,dry\,sand}\left(\rho_{drysand}-\rho_{o,drysand}\right) & \rho_{o,dry\,sand}\le\rho_{dry\,sand}\le\rho^{*}_{dry\,sand}\\ B_{SolidComp,dry\,sand}\left(\rho_{drysand}-\rho_{s,drysand}\right) & \rho_{dry\,sand}>\rho^{*}_{dry\,sand}\end{cases} \quad (4)$$

where $B_{Pl.Comp,\ dry\ sand}$ and $B_{SolidComp,\ drysand}$ (=21.68 MPa.m^3/kg [2])are respectively the plastic compaction (densification) and the solid-particle compaction moduli, while $\rho_{o,drysand}=(1-\alpha_0)\rho_{s,dry\,sand}$ and $\rho_{s,dry\ sand}$ (=2641 kg/m^3) are the initial density of dry sand and the density of the fully compacted sand, respectively and α_o denotes the initial porosity in sand. It should be noted, that the compaction moduli used in Eq. (4) are defined as a ratio of the corresponding bulk moduli and mass-densities. The plastic compaction modulus, $B_{Pl.Comp,\ dry\ sand}$, is defined as:

$$B_{Pl.Comp,dry\,sand}=\frac{P_{Comp,dry\,sand}}{\left(\rho^{*}_{dry\,sand}-\rho_{o,dry\,sand}\right)} \quad (5)$$

where $P_{Comp,\ dry\ sand}$ (=0.650GPa [13]) is the minimum pressure needed for full densification of sand and $\rho^{*}_{dry\ sand}$ is given by;

$$\rho^{*}_{dry\,sand}=\rho_{s,dry\,sand}+\frac{P_{Comp,dry\,sand}}{B_{SolidComp,dry\,sand}} \quad (6)$$

To account for the effect of clay in CU-ARL dry clayey sand (specifically that the volumetric-response is controlled by the more compliant clay layer over-coating sand particles), the CU-ARL dry sand EOS model parameters are generalized as:

$$\rho_{o,dry,clayey\,sand}=(1-\alpha)\rho_{s,dry\,clayey\,sand}=(1-\alpha)\left[(1-\Omega)\rho_{s,dry\,sand}+\Omega\rho_{s,clay}\right] \quad (7)$$

$$P_{Comp,dry\,clayey\,sand}=(1-\Omega)P_{Comp,dry\,sand}+\Omega P_{Comp,clay} \quad (8)$$

$$B_{Pl.Comp,dry\,clayey\,sand}=\frac{P_{Comp,dry\,clayey\,sand}}{\left(\rho^{*}_{dry\,clayey\,sand}-\rho_{o,dry\,clayey\,sand}\right)} \quad (9)$$

$$\rho^{*}_{dry\,clayey\,sand}=\rho_{s,dry\,clayey\,sand}+\frac{P_{Comp,dry\,clayey\,sand}}{B_{SolidComp,dry\,clayey\,sand}} \quad (10)$$

and

$$B_{Solid\ comp,dry\,clayey\,sand}=(1-\Omega)B_{Solid\ comp\,dry\,sand}+\Omega B_{Solid\ comp\,clay} \quad (11)$$

Saturated Sand: The (high deformation-rate) pressure vs. density curve for saturated clayey sand is defined as a simple extension of the pressure vs. density curve for saturated sand [2] and is expressed as:

$$P_{sat\,clayey\,sand}=\begin{cases}0 & \rho_{sat\,clayey\,sand}\le\rho_{o,sat\,clayey\,sand}\\ B_{sat\,clayey\,sand}\left(\rho_{sat\,clayey\,sand}-\rho_{o,sat\,clayey\,sand}\right) & \rho_{sat\,clayey\,sand}>\rho_{o,sat\,clayey\,sand}\end{cases} \quad (12)$$

where $B_{sat\ clayey\ sand}$ is the compaction modulus of saturated clayey sand and is defined using the compaction modulus of dry clayey sand, $B_{SolidComp,\ dry\ clayey\ sand}$ and the compaction modulus of water, B_w, and the fact that both the solid phase and the water-filled porosity form continuous networks, as:

$$B_{sat\,clayey\,sand}=(1-\alpha_0)B_{SolidComp,dry\,clayey\,sand}+\alpha_0 B_w \quad (13)$$

while $\rho_{o,\ sat\ clayey\ sand}$ is the initial density of saturated clayey sand and is defined in terms of the density of dry clayey sand, $\rho_{s,dry\ clayey\ sand}$, and the density of water, ρ_w, as:

$$\rho_{o,sat\,clayey\,sand}=(1-\alpha)\rho_{s,dry\,clayey\,sand}+\alpha\rho_w \quad (14)$$

Unsaturated Sand: The pressure vs. density curve for unsaturated clayey sand is obtained as a linear combination of the pressure vs. density relations for the dry clayey and the saturated clayey sands, as:

$$P_{unsat\,clayey\,sand}(\alpha_o,\beta,\Omega)=\begin{cases}0 & \rho_{unsat\,clayey\,sand}\le\rho_{o,unsat\,clayey\,sand}\\ B_{unsat\,clayey\,sand,low}\left(\rho_{unsat\,clayey\,sand}-\rho_{o,unsat\,clayey\,sand}\right) & \rho_{o,unsat\,clayey\,sand}\le\rho_{unsat\,clayey\,sand}\le\rho^*_{unsat\,clayey\,sand}\\ B_{unsat\,clayey\,sand,high}\left(\rho_{unsat\,clayey\,sand}-\rho^*_{unsat\,clayey\,sand}\right) & \rho_{unsat\,clayey\,sand}>\rho^*_{unsat\,clayey\,sand}\end{cases} \quad (15)$$

where

$$\rho_{o,unsat\,clayey\,sand}=(1-\beta)\rho_{o,dry\,clayey\,sand}+\beta\rho_{o,sat\,clayey\,sand} \quad (16)$$

$$\rho^*_{unsat\,clayey\,sand}=(1-\gamma_1)\rho^*_{dry\,clayey\,sand}+\gamma_1\rho^*_{sat\,clayey\,sand} \quad (17)$$

$$B_{unsat\,clayey\,sand,low}=\frac{P_{Comp\,dry\,clayey\,sand}}{\left(\rho^*_{unsat\,clayey\,sand}-\rho_{o,unsat\,clayey\,sand}\right)} \quad (18)$$

$$B_{unsat\,clayey\,sand,high}=\left[\frac{1}{\frac{(1-\beta)}{B_{SolidComp,dry\,clayey\,sand}}+\frac{\beta}{B_{sat\,clayey\,sand}}}\right] \quad (19)$$

where

$$\gamma_1=\beta\left[\frac{1-\frac{P_{Comp\,dry,clayey\,sand}}{B_{Sat\,clayey\,sand}\rho^*_{sat\,clayey\,sand}}}{(1-\beta)\left(1-\frac{P_{Comp\,dry\,calyey\,sand}}{B_{Pl.Comp,dry\,clayey\,sand}\rho^*_{dry\,clayey\,sand}}\right)+\beta\left(1-\frac{P_{Comp,dry\,calyey\,sand}}{B_{sat\,clayey\,sand}\rho^*_{sat\,clayey\,sand}}\right)}\right] \quad (20)$$

Eq. (19) reflects the fact that the compaction modulus of humid air residing in clayey sand, consisting of dry air and water, is dominated by its more compliant phase (dry air).

Eqs. (8)- (20) define the pressure vs. density relation during loading which results in (irreversible) compaction of clayey sand. During unloading/elastic-reloading the pressure vs. density relationship is nearly linear with the slope being equal to the (density-dependent) sound speed, *C*. Thus to fully define the CU-ARL clayey sand EOS model, a *C* vs. ρ relation must also be specified. The material sound speed is defined as a square-root of the ratio of the bulk modulus and the material mass density.

Dry Sand: The bulk modulus (in GPa) vs. density relationship for CU-ARL dry sand is given as [2]:

$$K_{drysand}=\begin{cases}0 & \rho_{drysand}<\rho_{o,drysand}\\ -15.6302+0.0094074\rho_{drysand} & \rho_{o,drysand}<\rho_{drysand}\le 0.8137\rho_{s,drysand}\\ -93.05+0.0455\rho_{drysand} & 0.8137\rho_{s,drysand}\le\rho_{drysand}\le 0.9837\rho_{s,drysand}\\ -1873.3+0.73074\rho_{drysand} & 0.9837\rho_{s,drysand}<\rho_{drysand}<\rho_{s,drysand}\\ -3.233+0.022651\rho_{drysand} & \rho_{drysand}>\rho_{s,drysand}\end{cases} \quad (21)$$

To account for the effect of clay in CU-ARL dry clayey sand, the CU-ARL dry sand bulk modulus is modified as:

$$K_{dry,clayey\,sand} = \left[\frac{1}{\frac{(1-\Omega)}{K_{drysand}\left(\rho_{dry\,sand}\right)} + \frac{\Omega}{K_{clay}}} \right] \tag{22}$$

where $K_{dry\,sand}$ is the bulk modulus of dry sand and K_{clay} is the bulk modulus of clay [17].

Saturated Sand: The density-dependent bulk modulus in saturated clayey sand is derived following the same procedure as in the case of P vs. ρ relation as:

$$K_{sat,clayeysand} = B_{sat,clayeysand}\,\rho_{sat,clayeysand} \tag{23}$$

Unsaturated Sand: Likewise, the density-dependent bulk modulus for unsaturated clayey sand is defined as:

$$K_{unsat,clayey}(\rho_{unsat,clayey}, \Omega, \alpha_o, \beta) = \left[(1-\beta)K_{dry,\,clayey\,sand} + \beta\, K_{sat,\,clayey\,sand}\right] \tag{24}$$

where

$$\rho_{dry,clayeysand} = \rho_{unsat,clayey\,sand} - \alpha_0 \beta \rho_{water} \tag{25}$$

and

$$\rho_{sat,clayeysand} = \rho_{unsat,clayey\,sand} + \alpha_0 (1-\beta)\rho_{water} \tag{26}$$

As mentioned earlier, the density dependent sound speed (for dry, saturated and unsaturated clayey sand) is defined as a square root of the ratio of the corresponding bulk moduli and mass densities.

To show the effect of clay on the EOS of sand, a comparison between the EOS relations for CU-ARL sand and CU-ARL clayey sand with 15vol. % of clay is made in Figures 2(a)-(b).

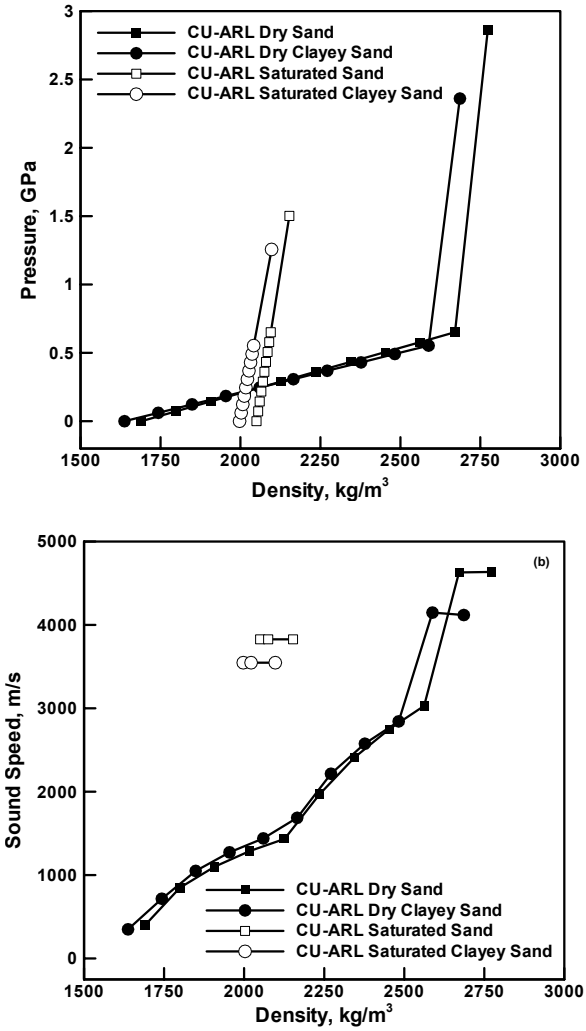

Fig.2 (a) Pressure vs. density and (b) sound speed vs. density relation for dry and saturated CU-ARL and CU-ARL clayey sand (15vol. % clay) with a porosity level of 36% at different degrees of saturation.

CU-ARL Clayey-sand Strength Model

Dry Sand: Since no inter-particle adhesion exists in dry sand, the following inter-particle friction-based, pressure dependent strength model for dry sand was defined within the CU-ARL sand model as [2]:

$$\sigma_{y,dry\,sand} = \begin{cases} \mu_{dry\,sand} P_{dry} & 0 < P_{dry} \le P_{MC} \\ \mu_{dry\,sand} P_{MC} & P_{dry} > P_{MC} \end{cases} \tag{27}$$

where $\mu_{dry\ sand}$ is the inter-particle friction coefficient for dry sand and is equal to 1.37 [13].

The presence of clay over-coat on the sand particles in expected to give rise to inter-particle adhesion while the inter-particle friction coefficient is expected to be reduced. Consequently, the pressure dependent yield strength for CU-ARL dry clayey sand can be defined as:

$$\sigma_{y,dry\,clayey\,sand} = \begin{cases} \sigma_{adhesion} + \mu_{dry\,clayey\,sand} P_{dry} & 0 < P_{dry} \le P_{MC} \\ \sigma_{adhesion} + \mu_{dry\,clayey\,sand} P_{MC} & P_{dry} > P_{MC} \end{cases} \tag{28}$$

where $\sigma_{adhesion}$ is the inter-particle adhesion and $\mu_{dry\ clayeysand}$ is the friction coefficient of dry clayey sand and, in order to account for the fact that inter-particle shear is controlled by the presence of clay, is defined as follows:

$$\mu_{dry\,clayey\,sand} = \frac{\mu_{dry\,sand}\mu_{clay}}{(1-\Omega)\mu_{clay} + \Omega\mu_{dry\,sand}} \tag{29}$$

where μ_{clay} (= 0.4599, [23]) is defined as the slope of the yield strength vs. pressure curve for dry clay.

Saturated Sand: The presence of water in saturated sand reduces the inter-particle friction coefficient and hence, the CU-ARL strength model for saturated sand was defined as:

$$\sigma_{y,sat} = \begin{cases} \mu_{sat\,sand} P_{sat} & 0 \le P_{sat} \le P_{MC} \\ \mu_{sat\,sand} P_{MC} & P_{sat} > P_{MC} \end{cases} \tag{30}$$

where the yield-stress-to-pressure proportionality coefficient, $\mu_{sat\,sand}$, is defined as:

$$\mu_{sat\,sand} = \begin{cases} 0.1 + \left(\mu_{dry\,sand} - 0.1\right)\dfrac{P_{sat}}{P_{MC}} & 0 \le P_{sat} \le P_{MC} \\ \mu_{dry\,sand} & P_{sat} > P_{MC} \end{cases} \tag{31}$$

in order to account for the effect of pressure on the inter-particle water-layer thickness (i.e. inter-particle friction coefficient). Similarly, to account for the presence of clay over-coat on the sand particles in clayey sand, Eq. (30) is modified as:

$$\sigma_{y,sat\,clayey\,sand} = \begin{cases} \sigma_{adhesion} + \mu_{sat\,clayey\,sand} P_{sat} & 0 \le P_{sat} \le P_{MC} \\ \sigma_{adhesion} + \mu_{sat\,clayey\,sand} P_{MC} & P_{sat} > P_{MC} \end{cases} \tag{32}$$

where the inter-particle friction coefficient for saturated clayey sand, $\mu_{sat\ clayey\ sand}$, is given by:

$$\mu_{sat\,clayey\,sand} = \begin{cases} 0.1 + \left(\mu_{dry\,clayey\,sand} - 0.1\right)\dfrac{P_{sat}}{P_{MC}} & 0 \le P_{sat} \le P_{MC} \\ \mu_{dry\,clayey\,sand} & P_{sat} > P_{MC} \end{cases} \tag{33}$$

Unsaturated Sand: The yield stress vs. pressure relationship for the unsaturated clayey sand can then be defined using a linear combination of the yield-stress/pressure proportionality coefficients in dry clayey and the saturated clayey sand as:

$$\sigma_{y,unsat\,clayey\,sand} = \begin{cases} \mu_{unsat\,clayey\,sand} P_{unsat} & 0 \le P_{unsat} \le P_{MC} \\ \mu_{unsatclayey\,sand}\ P_{MC} & P_{unsat} > P_{MC} \end{cases} \tag{34}$$

where

$$\mu_{unsat\,clayey\,sand} = (1-\beta)\,\mu_{dry\,clayey\,sand} + \beta\mu_{sat\,clayey\,sand} \tag{35}$$

The term P_{MC} appearing in Eqs. (27) - (35) is the Mohr-Coulomb pressure beyond which the yield stress is pressure insensitive and is defined as:

$$P_{MC} = (1-\Omega) P_{MC,dry\ sand} + \Omega P_{MC,dry\ sand} \frac{P_{Comp,Clay}}{P_{Comp,dry\ sand}} \tag{36}$$

where $P_{MC,dry\ sand}$ (=1.864.10^5 *kPa*) [2].

In addition to specifying the yield stress vs. pressure relationship, the compaction strength model entails the knowledge of the density dependent shear modulus. The shear modulus is used to define the relationship between the deviatoric stress and the deviatoric strain components during unloading/elastic reloading.

Dry Sand: The CU-ARL dry sand model shows a relatively modest initial increase in the shear modulus with an increase in density until the moment of full compaction, at which point, the shear modulus becomes a very sensitive function of density. This ($G_{dry\ sand}$ vs. $\rho_{dry\ sand}$) relationship can be found in our previous work [2]. To account for the fact that sand particles are coated with a continuous layer of clay the following rule of mixtures is used to define the shear modulus of dry clayey sand:

$$G_{dry,clayey\ sand} = \left[\frac{1}{\frac{(1-\Omega)}{G_{drysand}\left(\rho_{dry\ sand}\right)} + \frac{\Omega}{G_{dry\ clay}}} \right] \tag{37}$$

where the shear modulus of dry clay, $G_{dry\ clay}$ is typically equal to 6 GPa [24]. Eq. (37) is used as follows: From the current level of density of dry clayey sand:

$$\rho_{dry,clayey\ sand} = (1-\Omega)\rho_{dry\ sand} + \Omega\rho_{clay} \tag{38}$$

the density of the constituent dry sand, $\rho_{dry\ sand}$ is determined and used in the $G_{dry\ sand}$ vs. $\rho_{dry\ sand}$ relation to assess the $G_{dry\ sand}$ term. Next, $G_{dry\ sand}$ is used in Eq. (37) to compute $G_{dry\ clayey\ sand.}$

Unsaturated and Saturated Sand: Next, the effect of water on the shear modulus of unsaturated and saturated clayey sands is defined using a relation analogous to that given in Eq. (37) except that the $G_{dry\ clay}$ is replaced with the following expression:

$$G_{sat/unsat\ clay} = (1-\beta) G_{dry\ clay} \tag{39}$$

Similarly, the density of unsaturated/saturated clayey sand is defined as:

$$\rho_{sat/unsat\ clayey\ sand} = (1-\beta)\rho_{dry\ clayey\ sand} + \alpha\beta\rho_{water} \tag{40}$$

To show the effect of clay on the strength model of sand, a comparison between the strength models for CU-ARL sand and CU-ARL clayey sand with 15vol. % of clay is made in Figures 3(a)-(b).

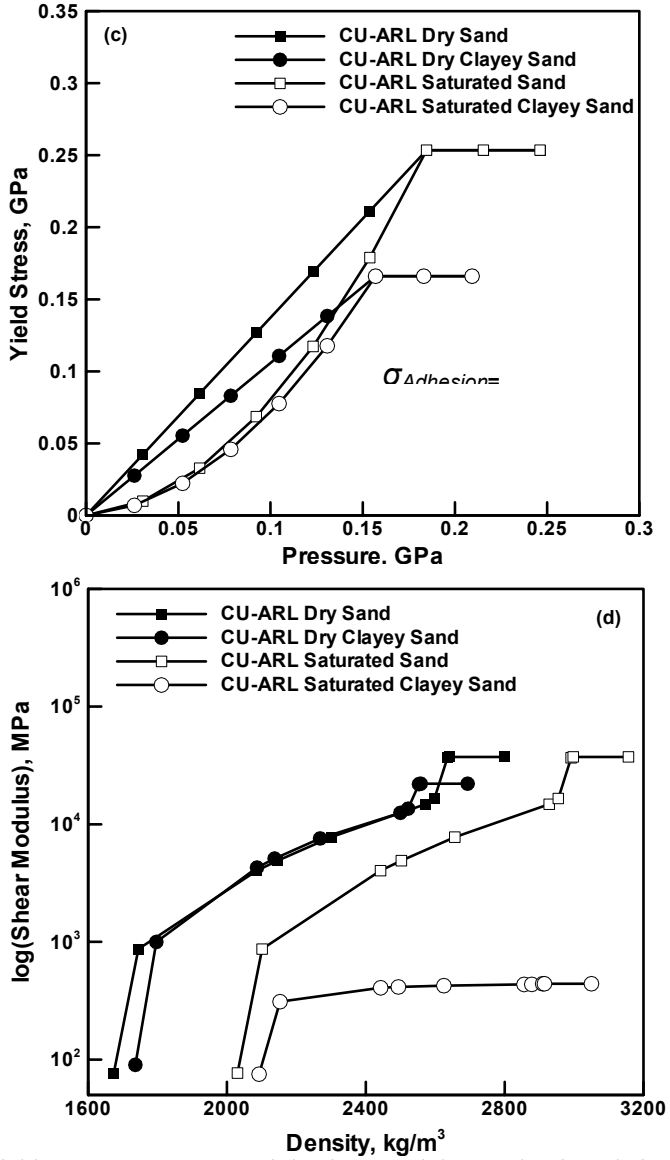

Fig.3 (a) Yield stress vs. pressure and (b) shear modulus vs. density relation for dry and saturated CU-ARL and CU-ARL clayey sand (15vol. % clay) with a porosity level of 36% at different degrees of saturation.

CU-ARL Clayey-sand Failure Model

The CU-ARL sand failure model developed in our previous work [2] is of a "*hydro*" type, according to which failure occurs when the negative pressure falls below a critical value, P_{fail}. After failure, the material looses the ability to support any tensile or shear loads but retains the ability to support compressive loads. To account for the experimentally observed fact that the failure pressure in sand at the saturation level of

0.75 is around 15%of that in saturated sand, the following saturation-level dependent failure pressure relation was proposed:

$$P_{unsatclayeysand,fail} = \beta^5 P_{fail.sat} \tag{41}$$

where $P_{fail,\ sat}$ for sand with a negligible amount of silt (which promotes the effect of capillarity and tension) is reported in Ref. [18] to be ca. 70 kPa. The CU-ARL sand failure model was adopted in Ref. [2] to account for the fact that failure in sand is more likely to take place by decohesion than by shearing. In clayey sand, however, one can expect that shear failure is more likely to take place than decohesion. For this reason, a hybrid "*hydro*" + "*shear*" failure model is adopted for the CU-ARL clayey sand. According to this model, failure will occur when one of the two conditions $P<P_{\text{fail}}$ or $\tau<\tau_{fail}$ is reached. To account for the effect of clay content and the effect of saturation on the failure resistance of clayey sand, the following relations are proposed:

$$P_{unsatclayeysand,fail} = (1-\Omega)\beta^5 P_{fail,sat} + \Omega\left[(1-\beta)P_{clay,fail} + \beta P_{fail,sat}\right] \tag{42}$$

$$\tau_{fail,claeysand} = \frac{\tau_{fail,clay}\tau_{fail,sat}}{(1-\Omega)\tau_{fail,clay} + \Omega\tau_{fail,sat}} \tag{43}$$

The CU-ARL parameters appearing in Eqs. (42) - (43) are listed in Table 2.

Table 2. Parameters appearing in the definition of the failure model for dry, unsaturated and saturated clayey sands.

Parameter	Symbol	Unit	Value
Saturated Sand			
Saturated Sand Tensile Failure Pressure	$P_{fail\ sat\ \mathbf{sand}}$	kPa	70
Saturated Sand Shear Failure Pressure	$\tau_{sat\ sand}$	kPa	350
Clay			
Clay Tensile Failure Pressure	$P_{fail\ clay}$	kPa	20
Clay Shear Failure Pressure	τ_{clay}	kPa	150

CU-ARL Clayey-sand Erosion Model

Erosion of a clayey-sand material element is assumed to take place when geometrical (i.e. elastic plus plastic plus damage/crack) instantaneous strain reaches a maximum allowable value. Our prior investigation [10] established that the optimal value for the geometrical instantaneous strain is ~1.0. When a material element is eroded, its nodes are retained along with their masses and velocities in order to conserve momentum of the system.

3. Validation of the CU-ARL Clayey-sand Model

The CU-ARL clayey sand model presented in Section II.3 was developed using simple physical arguments regarding the effects of moisture and minor contents of clay on the dynamic mechanical behavior of sand and parameterized using various material testing results. In this section, an attempt is made to validate the CU-ARL clayey sand model by comparing the available experimental results pertaining to the detonation of shallow-

buried landmines in clayey sand with the corresponding transient non-linear dynamics simulations of the same experiments. In order to assess the potential improvements in modeling the behavior of clayey sand, simultaneous non-linear dynamics simulations were also carried out using the original CU-ARL sand model. Such simulations are carried in the present work using the commercial software AUTODYN [11]. A brief description of the basics of a typical transient non-linear dynamics analysis is discussed in the next section.

3.1 Basics of Transient Non-Linear Dynamics Simulations

A transient non-linear dynamics problem is analyzed within AUTODYN [11] by solving simultaneously the governing partial differential equations for the conservation of momentum, mass and energy along with the materials constitutive equations and the equations defining the initial and the boundary conditions. The equations mentioned above are solved numerically using a second-order accurate explicit scheme and one of the two basic mathematical approaches, the Lagrange approach and the Euler approach. Within AUTODYN these approaches are referred to as "*processors*". The key difference between the two basic processors is that within the Lagrange processor the numerical grid is attached to and moves along (and deforms) with the material during calculation while within the Euler processor, the numerical grid is fixed in space and the material moves through it. In our recent work [2], a brief discussion was given of how the governing differential equations and the materials constitutive models define a self-consistent system of equations for the dependent variables (nodal displacements, nodal velocities, cell material densities and cell internal energy densities).

In the present work, both the Lagrange and Euler processors are used. The Lagrange processor was used to model the sand and various targets and structural components. High-energy explosives, gaseous mine-detonation products and the surrounding air are modeled using either a single-material FCT (Flux Corrected Transport) or a multi-material Euler processor. Different regions of the mine/air/target/sand model are allowed to interact and self-interact using the AUTODYN interaction options. A brief overview of the parts interactions and self interaction AUTODYN algorithms can be found in our recent work [2]. Also a detailed description of the Lagrange, Euler-FCT and multi-material Euler processors as well as of the material models used for air, high explosives and metallic structural materials can be found in our recent work [1,2].
Throughout this manuscript, the terms "*Depth of Burial*" (DOB) and the "*Stand-off Distance*" (SOD) are used to denote distances between the mine top face and the sand/air interface and between the sand/air interface and the bottom face of the target structure, respectively.

In the remainder of the manuscript, a separate comparison between the computational and experimental results are presented for the total blast-induced momentum transferred to the target and for the spatial and temporal evolution of the sand overburden bubble and the associated pressure fields.

3.2 Total Momentum Transferred to the Target Structure

To assess the ability of the CU-ARL clayey sand model to account for the total momentum transferred to the target structure following detonation of a ground-laid or shallow buried mine at different saturation levels of the sand and different contents of

clay, the computational results are compared with their experimental counterparts obtained in Refs. [14, 16].

3.2.1 Dry and Unsaturated Clayey Sand

To assess the ability of the CU-ARL clayey sand model to account for the total momentum transferred to the target structure at different levels of clay content and at low to medium saturation levels, a non-linear dynamics based computational analysis of the interaction of detonation products, mine fragments and sand ejecta with an instrumented horizontal mine-impulse pendulum used in Ref. [16], is carried out and the computed results compared with their experimental counterparts. In this section, a brief overview of the- construction and experimental procedure associated with the impulse pendulum is first presented.

The instrumented horizontal mine-impulse pendulum, as shown in Figure 4, consists of a 5m long horizontal steel arm with a 1200mm x 1200mm square measuring pan placed at the free end of the arm 400mm above the ground. The arm is attached to the base assembly at the other end through a horizontal pivot. The charge, typically consisting of a cylindrically shaped (14.6cm in diameter and 5cm high) C4 mine is placed under the center of the measuring pan and detonated. The mine is either laid on the ground or is buried to different depths. The resultant maximum angular displacement of the pendulum arm is measured and used to calculate the detonation-induced impulse on the pendulum. The use of the mine-impulse pendulum enabled an investigation of the effects of the sand type/properties, extent of saturation with water, the extent of clay content, the target stand-off distance and the mine depth of burial on the total detonation-induced impulse. In an earlier design, the measuring pan was constructed of mild steel, however, the initial experiments revealed that such a measuring pan undergoes substantial plastic deformation. Consequently, the central 600mm x 600mm section of the measuring pan was replaced with a 50mm thick Rolled Homogenized Armor (RHA) plate. The maximum angular deflection of the pendulum was obtained using a combination of the following three methods: (a) a cable potentiometer, (b) a scratch gage and (c) a high speed video recording of a large pointer.

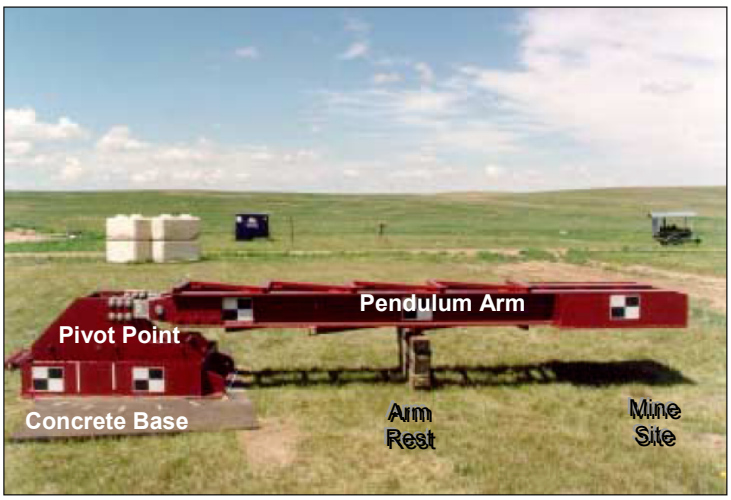

Fig.4 Horizontal Mine Impulse Pendulum (MIP) used in Ref [16].

Next, a brief description is given of the computational model used to simulate the interaction of the detonation-products/soil ejecta resulting from the explosion of a shallow-buried or ground-laid mine and the instrumented horizontal mine-impulse pendulum. The computational modeling of this interaction involved two distinct steps: (a) geometrical modeling of the instrumented horizontal mine-impulse pendulum and (b) a non-linear dynamics analysis of the momentum transfer from the detonation-products/soil ejecta to the pendulum.

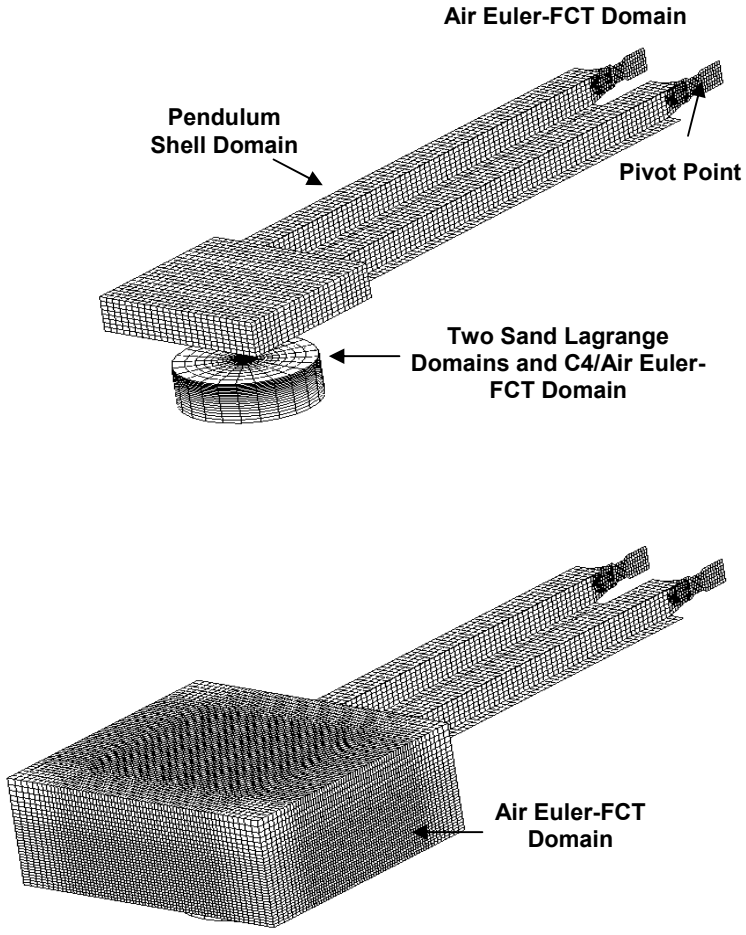

Fig.5 Various Computational domains used in the present non-linear dynamics analysis of the interactions of the detonation products, mine fragments and sand ejecta with the horizontal mine-impulse pendulum.

Various computational domains used in the present study are shown in Figure 5. The geometrical models for the various components of the pendulum were constructed using 50mm x 50mm square shell elements. An advantage was taken of the planar symmetry of the model. In other words, a vertical plane of symmetry was placed along the length of the pendulum which enabled only a half of the pendulum to be modeled. In

accordance with the instrumented horizontal mine-impulse pendulum used in Ref. [16], different sections of the pendulum were constructed using AISI 1006 steel and (Rolled Homogenized Armor) RHA plate material. Welded joints of the different sections of the pendulum were simulated by joining the components in question.

The head of the pendulum was placed in a single-material Euler-FCT region consisting of 74,000 25mm edge-length cubic cells. The Euler-FCT processor is a single material processor in which different materials are represented by a single material model derived using a Flux Corrected Transport (FCT) approach. The Euler-FCT processor was used in place of a multi-material Euler processor in order to reduce the computational cost. Many investigations (e.g. [1, 2]) showed that the Euler-FCT processor yields results which are quite comparable to their multi-material Euler counterparts. The landmine is modeled using the following procedure: In the case of a surface laid mine, the mine was represented by a high-density high-energy cylindrical air region located within the Euler-FCT domain. In the case of a shallow-buried mine, two joined Lagrange domains were used to define a sand region containing a cylindrical cavity whose shape and size match those of the C4 mine. A second Euler-FCT domain overlapping with the two sand domains is defined and the portion of this domain corresponding to the cylindrical sand cavity defined above is initially filled with high-density high-energy air.

The air/clayey sand and air/pendulum interactions are accounted for using the appropriate Euler/Lagrange coupling option with AUTODYN [11]. Likewise, the sand/pendulum interactions were modeled through the use of the appropriate Lagrange/Lagrange coupling option.

At the beginning of the simulation, the pendulum is assumed to be at rest (with the gravitational force acting downwards), while the Lagrange and Euler-FCT domains are filled with stationary materials (sand and air, respectively). The C4 mine was initially modeled as a cylindrical high-density, high-energy sub-domain within the Euler-FCT region.

The motion of the pendulum was constrained to within a vertical plane and a fixed single-point constraint was applied to its pivot point. The *"flow out"* boundary conditions were applied to all the free faces (the faces which do not represent interfaces between the different domains) of the Euler-FCT domain except for the face associated with the vertical symmetry plane. To reduce the effect of reflection of the shock waves at the outer surfaces of the Lagrange domain, *"transmit"* boundary conditions were applied to all the free faces of this domain except for the face associated with the vertical symmetry plane.

To speed up the calculations, all Euler-FCT and Lagrange domains were removed from the analysis after approximately 10ms following detonation when the extent of interaction between the detonation-products/sand ejecta and the pendulum was negligibly small.

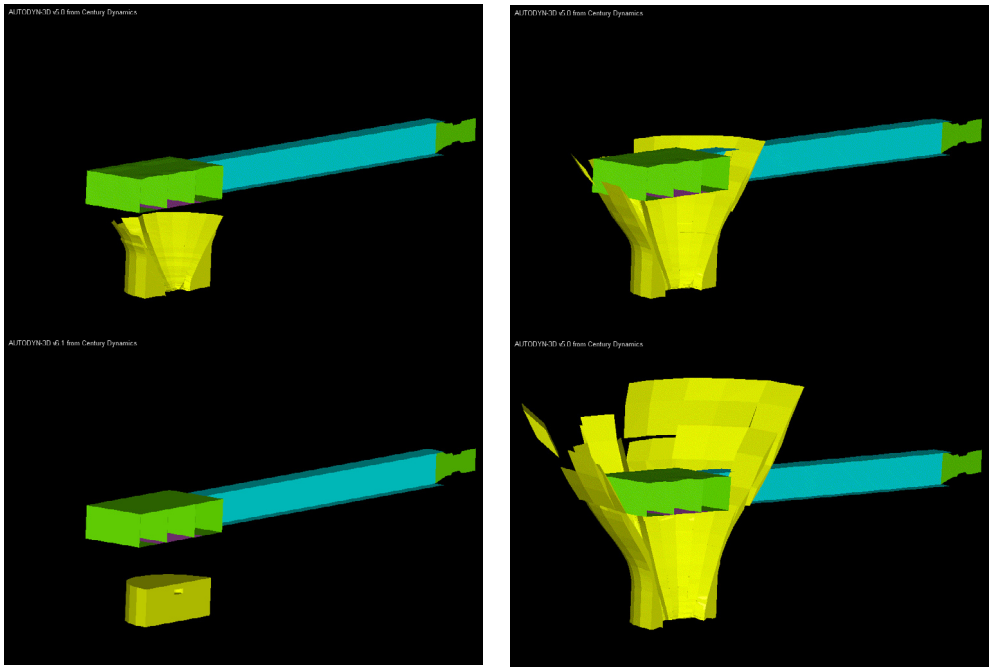

Fig.6 Temporal evolution of the material involved in the horizontal impact pendulum experiment post-detonation times: (a) 0ms; (b) 21ms; (c) 42ms and (d) 65ms.

A standard mesh sensitivity analysis was carried out (the results not shown for brevity) in order to ensure that the results obtained are insensitive to the size of the cells used.
The effect of the degree of (water) saturation in clayey sand with 15vol.% of clay [16] on the total impulse transferred to the pendulum in the case of sand containing various levels of moisture for four different DOBs of an 1kg C4 landmine is displayed in Figures 7(a)-(d). The 0cm-DOB corresponds to a *"flush-buried"* mine while the -5cm-DOB corresponds to a *"ground-laid"* mine.

An example of the temporal evolution of the distribution of materials involved in the horizontal mine impulse pendulum analysis is displayed in Figures 6(a)-(d). It should be noted that only one (longitudinal) half of the computational model is displayed for clarity.

A comparison of the experimental and computational results pertaining to the total impulse transferred to the instrumental horizontal mine-impulse pendulum at different levels of sand saturation with water at four different values of the depth of burial are displayed in Figures 7(a)-(d). To assess the extent of the potential agreement-improvement with the experimental results obtained by the use of the CU-ARL clayey sand model, the results obtained using the CU-ARL sand model are also displayed in Figures 7(a)-(d).

The results displayed in Figures 7(a)-(d) show that, at all the levels of saturation and for all four values of the DOB, the CU-ARL clayey sand model improves somewhat the agreement with the experimental results over that obtained in the case of CU-ARL sand model. However, the overall agreement between the experimental and the present

calculation results remains only fair. It should be noted that the experimental results are associated with substantial scatter rendering the CU-ARL clayey sand model validation quite difficult.

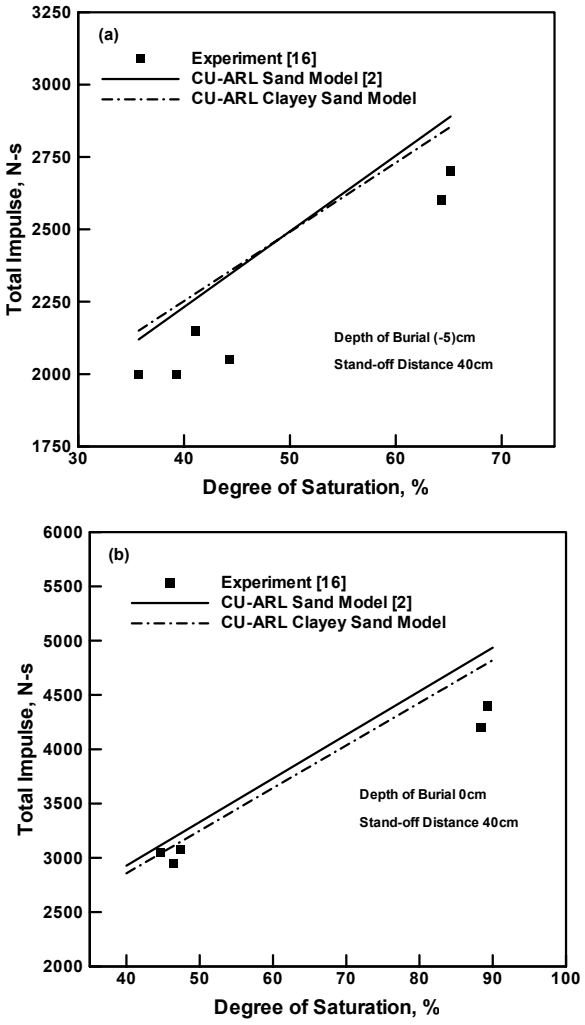

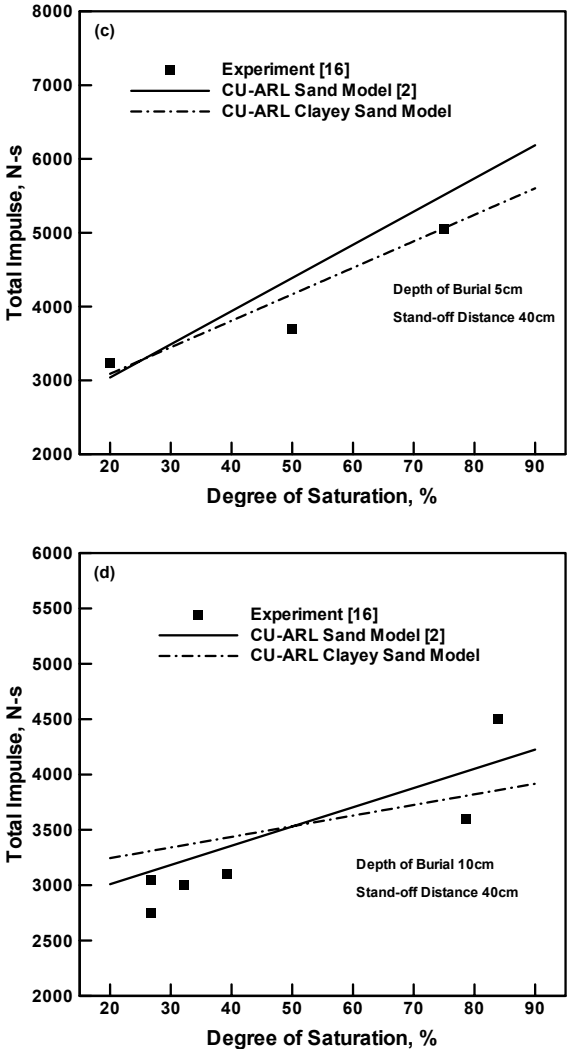

Fig.7 The effect of degree of saturation of CU-ARL and CU-ARL clayey sand on the total impulse transferred to the instrumented horizontal mine-impulse pendulum for the depths of burial of a) -5cm; b) 0cm; c) 5cm and d) 10cm.

3.2.2 Saturated Sand

To assess the ability of the CU-ARL clayey sand model to account for the total momentum transferred to the target structure at high saturation levels of the sand, a non-linear dynamics based computational analysis of the interaction of detonation products, mine fragments and sand ejecta with a Vertical Impulse Measurement Fixture used in Ref. [14] (Figure 8), is carried out and the computed results compared with their experimental counterparts. A brief overview of the construction and experimental procedure associated with the VIMF is presented first.

Fig.8 Vertical Impulse Measurement Fixture used in Ref [15].

Table 3. VIMF Set-Up and Test Conditions [14]

Test No.	Charge Mass kg	Charge Diameter m	Charge Height m	DoB* m	HoT** m	VIMF Target Total Mass kg
1+	4.54	0.254	0.56	0.10	0.40	12,506
3+	4.54	0.254	0.56	0.30	0.40	12,506
4+	4.54	0.254	0.56	0.10	0.20	12,506
4a++	4.54	0.254	0.56	0.10	0.20	11,852
5++	2.27	0.152	0.76	0.80	0	11,852
6++	4.54	0.254	0.56	0.10	0.40	11,852
7++	2.27	0.152	0.76	0.81	0.16	11,535
8++	7.47	0.236	0.86	0.10	0.40	11,535

* DoB = Depth of Burial
** HoT = Height of the Target plate above the soil
\+ Witness plate size: 2.43m by 2.82m by 0.088m
\++ Witness plate size: 1.83m by 3.65m by 0.088m

The VIMF is a structural mechanical device that enables direct experimental determination of the imparted blast-loading impulse via measurements of the vertical displacement of a known fixed-mass vertical guide rail that is capped with a witness plate, which serves as a momentum trap to capture the blast loading of the buried charge. The design and operation of the VIMF has been described in details by Gniazdowski et al. [19], and Skaggs et al. [20] and Taylor and Skaggs [14] and will be only briefly discussed here. To create the required water-saturated sand condition, a cylindrical pit 3.65m in diameter and 1.32m deep is first constructed in the soil within the VIMF test area. To retain water in the sand pit and to keep the sand-water mixture separate from the rest of the sand, the walls of the pit are lined with 0.32cm thick poly-ethylene sheets and the pit floor is built using a commercial swimming pool liner. Once the pit liners are in place, a series of water hoses is placed in pit bottom to allow the introduction of water into the pit from the bottom. Next, approximately 14.2m^3 of commercially available (Quickrete) sand is placed in the pit. The sand typically consists of 94.4wt.% sand, 0.3wt.% gravel, and 5.3wt.% clay. Prior to each test, water is allowed to fill the sand pit until standing water is observed on top of the sand.

The basic formulation of the computational problem dealing with the interactions between the detonation products, shell fragments and soil ejecta (all resulting from the explosion of a shallow-buried landmine) and the VIMF is presented next. The computational modeling of this interaction involved two distinct steps: (a) geometrical modeling of the VIMF along with the adjoining mine, air and sand regions, and (b) the associated transient non-linear dynamics analysis of the impulse loading (momentum transfer) from the detonation products, shell fragments and soil ejecta to the VIMF structure. The part (b) of this analysis was performed using a modified version of the technique developed by Fairlie and Bergeron [21]. This technique couples a multi-material Eulerian mesh to three Lagrangian meshes. The Eulerian mesh contained initially a TNT mine (and after mine explosion the resulting high-pressure, high-internal energy-density detonation products) and the (initially stationary, atmospheric-pressure) air. The mesh was constructed in terms of eight node elements. One of the Lagrangian mesh was used to model the soil, the other to represent the VIMF witness plate while the third one was used to model the remainder of the VIMF structure. The soil and the VIMF structure were modeled using eight node solid elements, while the witness plate was modeled using four-node shell elements.

An advantage was taken of the inherent symmetry of the model. In other words, two mutually-orthogonal vertical planes of symmetry were placed along the axis of the VIMF as well as along the axis of the air, mine and sand regions which enabled only a quarter of the computational model to be analyzed. Representative quarter symmetric models for various computational domains used in the present study are shown in Figure 9. It should be noted that the lower portion of the Eulerian domain contains the landmine while the rest of the lower portion of the Eulerian domain is occupied by the Lagrangian soil mesh. Likewise, the upper portion of the Eulerian domain which extends above the soil contains initially air and is partially occupied by the Lagrangian VIMF witness-plate and vertical-base meshes.

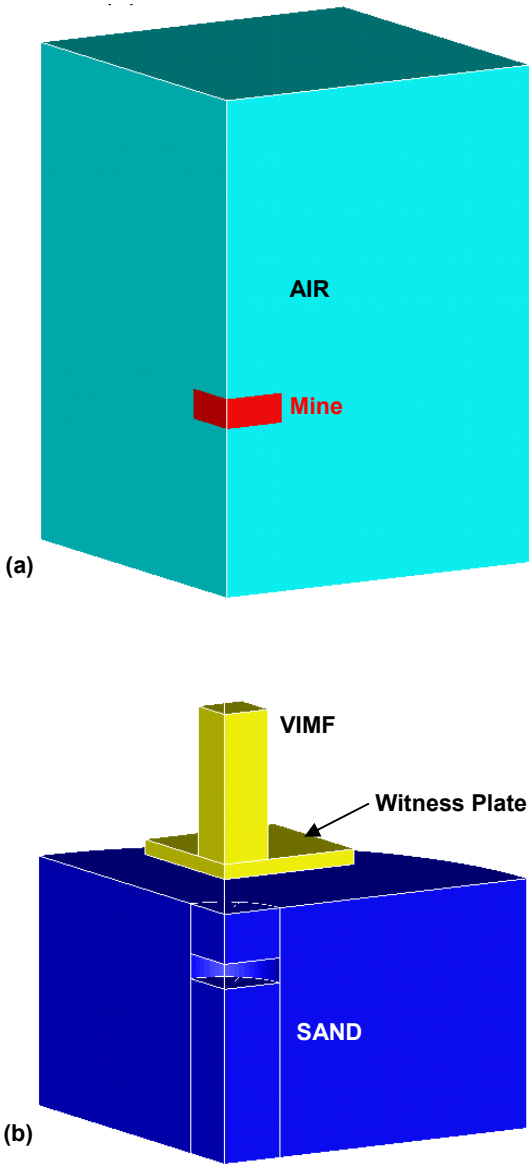

Fig.9 Various Computational domains used in the present non-linear dynamics analysis of the interactions of the detonation products, mine fragments and sand ejecta with the VIMF.

At the beginning of the simulation, all the Lagrange and Euler domains were activated and the landmine detonated. The (circular-disk shape) mine was detonated over its entire bottom face at the beginning of the simulation.

A standard mesh sensitivity analysis was carried out (the results not shown for brevity) in order to ensure that the results obtained are insensitive to the size of the cells used.

A comparison between the experimental and the computational results (based both on the use of the CU-ARL sand model and CU-ARL clayey sand model) pertaining to the

total impulse transferred to the VIMF are shown in Table 4. It should be remembered that all the results displayed in this table correspond to the fully saturated sand. The results displayed in Table 4 suggest that in all but one case (case 4) the CU-ARL clayey sand-model based results are in better agreement with their experimental counterparts relative to those between CU-ARL sand and the experimental results.

Table 4. Measured and Computed Impulse Transferred to the VIMF Witness Plate

Test No.	Measured Total Impulse (N-s)	Computed Total Impulse CU-ARL Sand Model (N-s)	Computed Total Impulse CU-ARL Clayey Sand Model (N-s)
1	71,801	78,014	74,673
3	74,017	64,561	63,656
4	81,125	83,622	95,342
4a	69,644	57,174	66,868
5	77,612	72,448	74,507
6	59,286	64,452	54,582
7	36,938	37,689	34,007
8	94,390	86,042	86,900

3.3 Spatial and Temporal Evolution of Sand-overburden Bubble and Pressure Fields

To farther assess the validity of the CU-ARL clayey sand model to account for the spatial and temporal evolutions of the sand-overburden bubble and the pressure fields, following detonation of a ground-laid or shallow buried mine at different saturation levels of the sand, the computational results are compared with their experimental counterparts obtained in Ref. [22]. In this section, a brief overview of the experimental set-up and the procedure used in Ref. [22] is first presented.

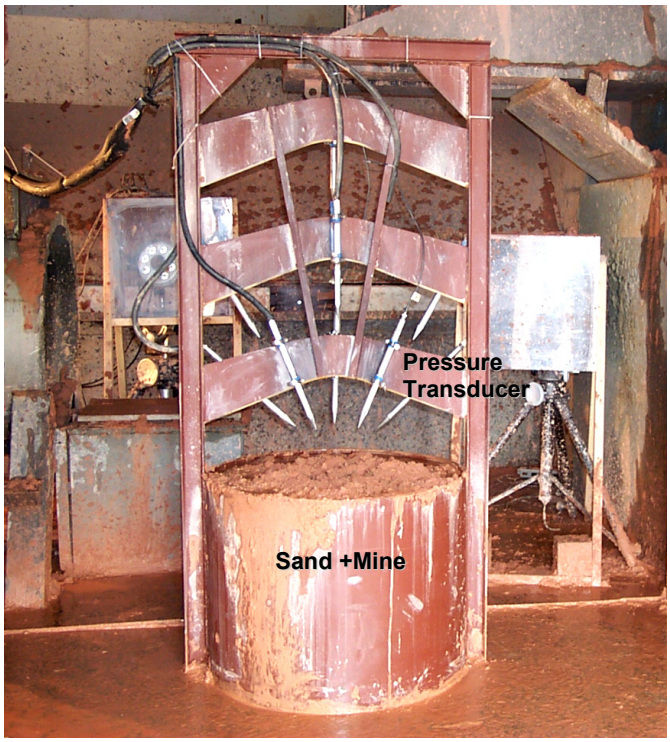

Fig.10 The experimental setup used in Ref. [22] to study the effect of explosion of a shallow-buried mine.

The experiments carried out in Ref. [22] can be briefly described as follows: A 1.27cm wall thickness cylindrical barrel with the outer-diameter of 81.6cm and the overall height of 71cm is filled with sand up to its top. A 100g cylindrical-disk shape C4 high-energy explosive (6.4cm in diameter and 2cm in height) is buried into the sand along the centerline of the barrel with its faces parallel with the sand surface. The Depth of Burial (DOB) (defined as the vertical distance between the top face of the explosive and the sand surface) is varied in a range between 0 and 8cm. Thus a 0cm DOB case corresponds to a flush-buried explosive. A set of six pressure transducers is utilized to monitor the pressure in the air following the detonation of the explosive. The first number in the Pressure Transducer (PT) designation represents the distance in centimeters of the transducer from the origin of the coordinate system (defined below), while the second number represents the angular relation in degrees between the position vector of the pressure transducer and the axis of symmetry. The location of the six pressure transducers is also shown in Figure 11. To be consistent with the definition of coordinate system for the 2D axi-symmetric problem used in AUTODYN [11], the y coordinates are measured in the radial direction from the centerline of the barrel, while the x coordinates are measured along the axis of symmetry, with $x=0$ corresponding to the sand surface and $x<0$ denoting the air region above the ground.

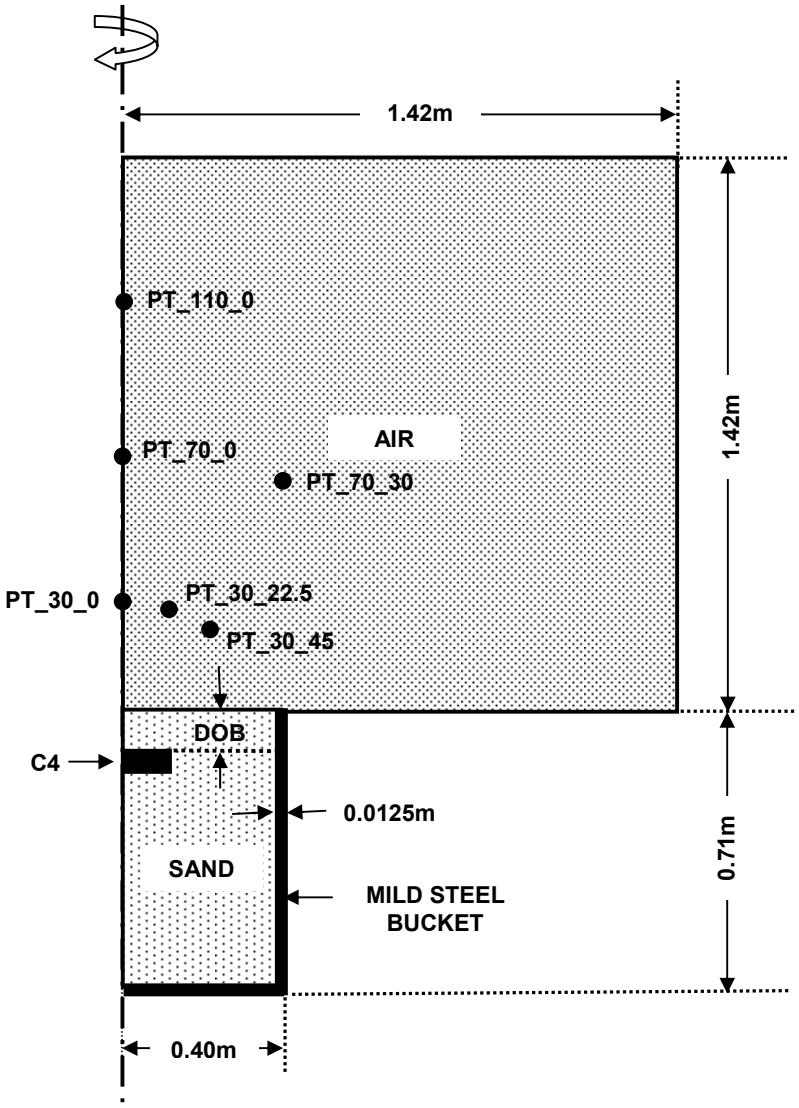

Fig.11 A simple schematic of the experimental setup used in Ref. [22] to study the effect of explosion of a shallow-buried mine.

The physical model displayed in Figure 11 has been represented using the computational multi-material Euler model shown in Figure 12. In Figure 12, various portions of the computational domain are filled with one or more of the attendant materials (air, sand, C4 gaseous-detonation products and AISI 1006 mild steel). Due to the inherent axial symmetry of the set-up used in Ref. [22], the mine detonation is analyzed as a 2D axi-symmetric problem. The left boundary in Figure 12 coincides with the axis of symmetry (x-axis). The horizontal direction (y-axis) corresponds to the radial direction.

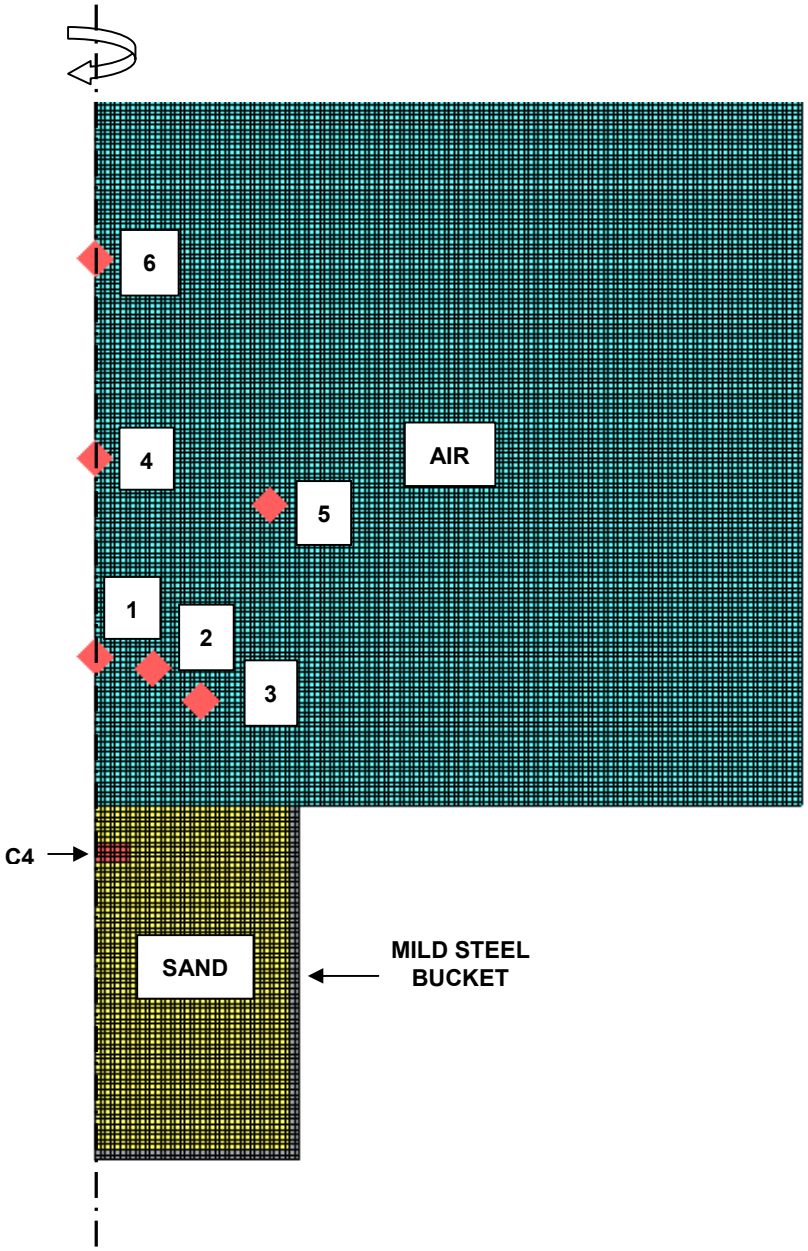

Fig.12 Computational sub-domains representing the experimental setup used in Ref. [22] to study the effect of explosion of a shallow-buried mine.

The *"flow-out"* boundary conditions are applied to all the outer boundaries of the computational domain. To mimic the detonation initiation conditions used in Ref. [22], detonation is initiated at the central circular portion of the explosive of radius 3.2cm, at the bottom face of the mine. To monitor the temporal evolution of pressure in air, six

gage points are introduced whose locations coincide with those of the pressure transducers used in Ref. [22].

A standard mesh sensitivity analysis was carried out (the results not shown for brevity) in order to ensure that the results obtained are insensitive to the size of the cells used.

A comparison between the computational results obtained in the present work and their experimental counterparts [22] as well as their CU-ARL sand model-based computational results [2] for the case of dry and saturated clayey sand are displayed in Figures 13(a)-(d) and 15(a)-(d), respectively. The results pertaining to the dry clayey sand will be discussed first.

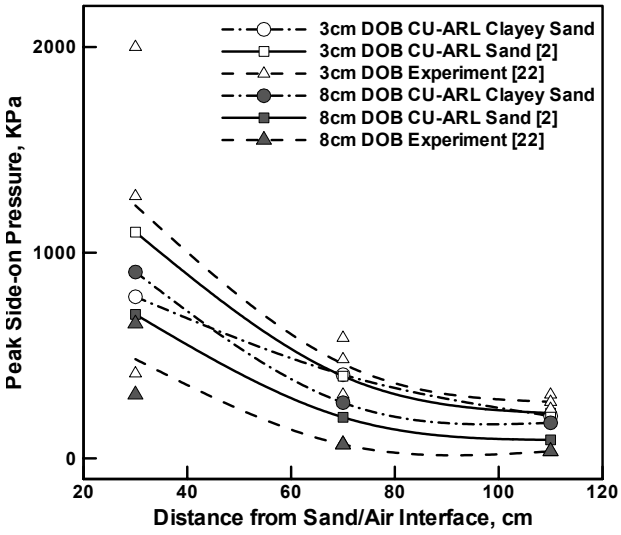

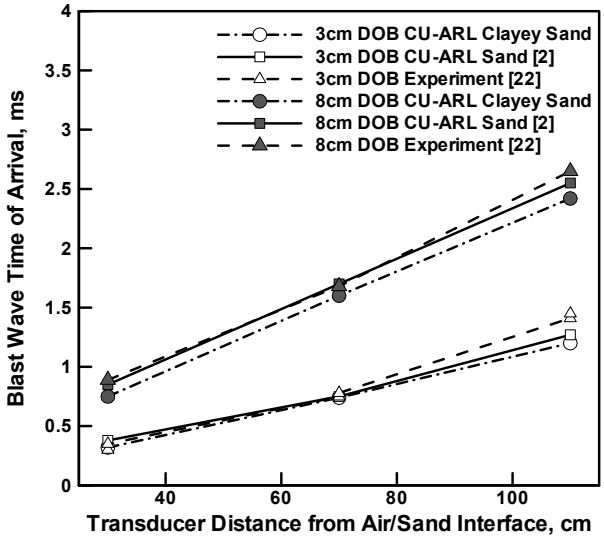

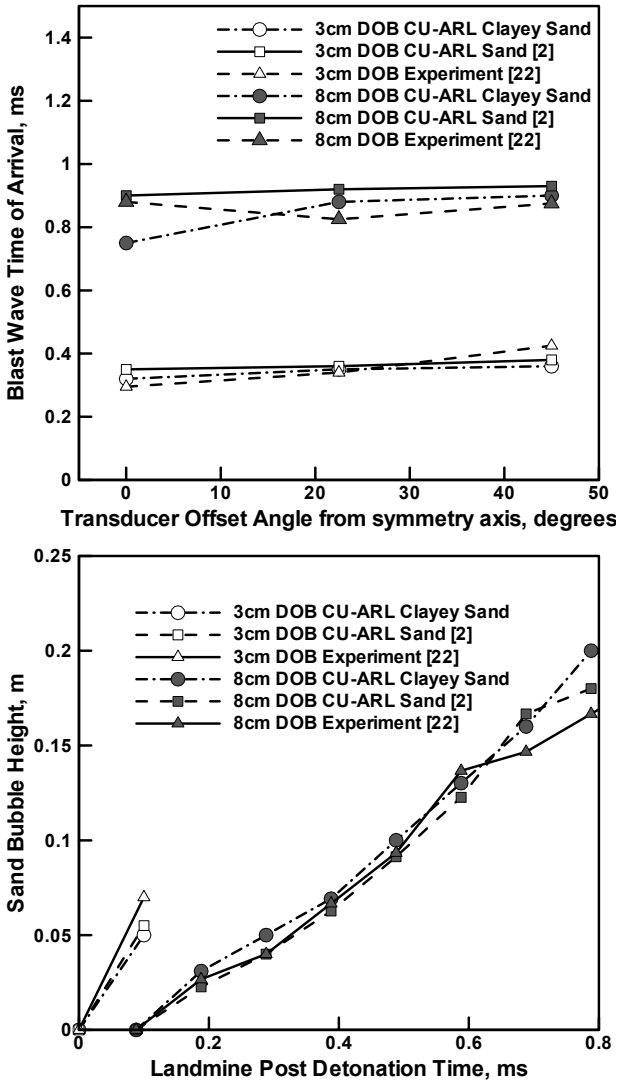

Fig.13 A comparison of the experimental [22] and computed (present work) results pertaining to various phenomena associated with landmine detonation in dry sand: (a) Side-on overpressure vs. transducer distance from air/sand interface; (b) Blast wave arrival time vs. transducer distance from air/sand interface; (c) Blast wave arrival time vs. transducer offset angle from the symmetry axis and (d) Sand bubble height vs. landmine post-detonation time.

The variation of the peak side-on (static) pressure in air with the distance (along the vertical axis) from the sand/air interface at two (3cm and 8cm) DOBs is displayed in Figure 13(a). The results displayed in Figure 13(a) show that at larger (>60cm) distances, the CU-ARL clayey sand model clearly shows improved agreement with the experiment over the CU-ARL sand model. At the shorter (30cm) distance, the experimental results

show excessive scatter so that a sensible computation-to-experiment quantitative comparison can not be carried out.

The variation of the blast-wave time of arrival with the distance from the sand/air interface at the same two DOBs is displayed in Figure 13(b). A simple analysis of the results displayed in this figure reveals that the agreement between the CU-ARL sand model-based results with the experimental results was already quite good and that level of agreement has not been significantly improved (or worsened) when the CU-ARL model was used.

The variation in the blast-wave time of arrival with offset angle (from vertical axis) at a fixed (30cm) distance from the sand/air interface is displayed in Figure 13(c). The results displayed in this figure show that with the exception of 8cm DOB and zero offset angle, the CU-ARL clayey sand model either improves agreement with the experiment or does not worsen it significantly.

The temporal evolution of the sand bubble height for the cases of 3cm and 8cm DOB is displayed in Figure 13(d). The results displayed in this figure show that both the CU-ARL and the CU-ARL clayey sand model yield a reasonable and comparable agreement with the experiment.

The computational results and their comparison with the experiment in the case of saturated sand are discussed next.

The results displayed in Figure 14(a) show that, in general, the CU-ARL clayey sand model worsens somewhat the agreement with the experimental relative to that observed for the CU-ARL sand. More specifically, the CU-ARL clayey sand model predicted peak pressures are on a higher side. This observation was found to be mainly affected by the choice of the value of the shear modulus of fully –saturated clay (a parameter whose mean value is associated with a considerable mount of uncertainty) in the strength part of the CU-ARL sand model.

The variation of the blast-wave time of arrival with the distance from the sand/air interface at the same two DOBs is displayed in Figure 14(b). A simple analysis of the results displayed in this figure reveals that the CU-ARL clayey sand model either improves agreement with the experiment (especially in the case of 8cm DOB) or does not worsen it significantly.

The variation in the blast-wave time of arrival with offset angle (from vertical axis) at a fixed (30cm) distance from the sand/air interface is displayed in Figure 14(c). The results displayed in this figure show that except for the case of 3cm DOB with no offset the CU-ARL clayey sand model either improves agreement with the experiment (especially in the case of 8cm DOB) or does not worsen it significantly.

The temporal evolution of the sand bubble height for the cases of 3cm and 8cm DOB is displayed in Figure 14(d). The results displayed in this figure show that both the CU-ARL and the CU-ARL clayey sand model yield a reasonable and comparable agreement with the experiment with the CU-ARL clayey sand performing better at later times in the computation cycle.

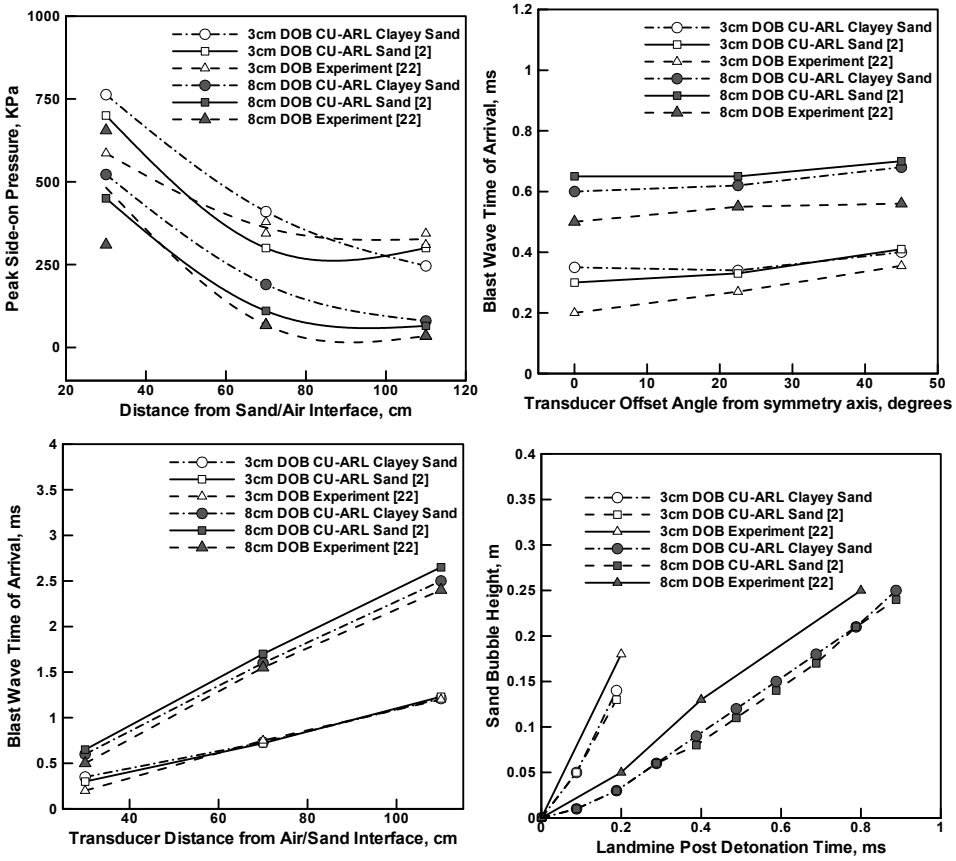

Fig.14 A comparison of the experimental [22] and computed (present work) results pertaining to various phenomena associated with landmine detonation in fully saturated sand: (a) Side-on overpressure vs. transducer distance from air/sand interface; (b) Blast wave arrival time vs. transducer distance from air/sand interface; (c) Blast wave arrival time vs. transducer offset angle from the symmetry axis and (d) Sand bubble height vs. landmine post-detonation time.

4. Summary and Conclusions

Based on the results obtained in the present work, the following main summary remarks and conclusions can be drawn:

1. Using a simple procedure based on a physics-based analysis and parameter estimation, the previously developed CU-ARL clay-free material model has been expanded to include the effects of clay, as well as the effects of water content.
2. The resulting CU-ARL clayey sand model was tested by comparing the computational results with their experimental counterparts for a number of investigations involving detonation of a landmine (buried in sand) and the interactions of the mine fragments, detonation products and sand ejecta with various target structures.

3. The comparison between the experimental and the computational results (those based on CU-ARL sand model and the CU-ARL clayey sand model) revealed that the CU-ARL clayey sand model shows somewhat better agreement with the experiment. However, in many cases the agreement remained only fair.

Acknowledgements

The material presented in this paper is based on work supported by the U.S. Army/Clemson University Cooperative Agreements W911NF-04-2-0024 and W911NF-06-2-0042 and by the U.S. Army Grant Number DAAD19-01-1-0661. The authors are indebted to Dr. Fred Stanton for the support and a continuing interest in the present work.

References:

[1]. M. Grujicic, B. Pandurangan and B. Cheeseman, *Shock Vibr.*, 13(2006)41-61.
[2]. M. Grujicic, B. Pandurangan, B. A. Cheeseman and W. N. Roy, *Shock Vibr.*, submitted for publication, (2006).
[3]. I. V. Gruhn, I*GCC Brief*, 6(2006).
[4]. M. P. M. Rhijnsburger, *11th International Symposium on Interaction of Effects of Munitions with Structures,* 2003.
[5]. Centers for Disease Control (CDC), *Morbidity and Mortality Weekly Report,* 46(1997)724-726.
[6]. K. R. Housen, K. A. Holsapple and R. M. Schmidt, *Journal of Geophysical Research*, 88(1983)2485-2499.
[7]. P. S. Westine, B. L. Morris, P. A. Cox and E. Polch, *Contract Report No. 1345, for U.S. Army TACOM Research and Development Center*, 1985.
[8]. B. L. Morris, *Final Report for Contract No. DAAK70-92-C-0058 for the U.S. Army Belvoir RDEC*, 1993.
[9]. D. Bergeron, S. Hlady and M. P. Braid, *17th International MABS Symposium*, 2002.
[10]. M. Grujicic, B. Pandurangan and B. Cheeseman, *MMMS.*, accepted for publication, 2006.
[11]. *AUTODYN-2D and 3D, Version 6.1, User Documentation,* 2006.
[12]. D. Bergeron, R. Walker and C. Coffey, *Suffield Report No. 668, Defence Research Establishment Suffield, Ralston*, Alberta, 1998.
[13]. P. Laine and A. Sandvik, *Proceedings of the 4th Asia-Pacific Conference on Shock and Impact Loads on Structures*, (2001)361-368.
[14]. L. C. Taylor, R. R. Skaggs and W. Gault, *Fragblast*, 9(2005)19-28.
[15]. M. Grujicic, B. Pandurangan, B. A. Cheeseman, W. N. Roy and R. R. Skaggs, *Journal of Materials: Design and Applications*, accepted for publication, 2006.
[16]. D. Bergeron, J. E. Tremblay, *16th International MABS Symposium*, 2000.
[17]. K. T. Spikes and J. P. Dvorkin, *The Leading Edge,* (2005)581-583.
[18]. S. Stein and T. Kim, *Marine Geosources and Geotechnology*, 22(2004)33-47.
[19]. N. Gniazdowski, *ARL Technical Report (in submission)*, 2004.
[20]. R. R. Skaggs, J. Watson, T. Adkins, W. Gault, A. Canami and A. D. Gupta, *ARL Technical Report (in submission)*
[21]. G. Fairlie and D. Bergeron, *Proceedings of the 17th Military Aspects of Blast Symposium*, 2002.
[22]. J. Foedinger, *SBIR Phase-II Plus Program, Technical Interchange Meeting,* 2005.
[23]. M .K. Jafari and A. Shafiee, *Canadian Geotechnical Journal*, 41(2004)1152-1167.
[24]. M. W. Lee, *Geophysical Prospecting*, 54(2006)177-185.